Convective heat transfer coefficient in air/liquid-water/ice/solid-wall multi-phase system

Kazuto Ueno* and Masoud Farzaneh
NSERC/Hydro-Quebec/UQAC Industrial Chair on Atmospheric Icing of Power Network Equipment (CIGELE) and Canada Research Chair on Atmospheric Icing Engineering of Power Networks (INGIVRE), www.cigele.ca
Université du Québec à Chicoutimi, Chicoutimi, QC, Canada
*Email: kazuto.ueno@uqac.ca

Abstract: The physical model currently used in ice accretion codes is based on the conservation of energy and mass within numerical cells along the ice-accreting surface. This type of model works reasonably well in rime icing conditions. However, the results are much less satisfactory in glaze icing conditions because the interaction between the air flow and the unfrozen surface water dynamics is neglected. Although the surface film flow generates a rough ice surface, almost all glaze icing models lack the physical motivation for the ice surface roughness. Instead, roughness is treated as an input parameter in the model. In this paper, we consider a physical model of the water film flow over a rough ice surface on an aluminum substrate, taking into account the interaction between the air and water flows. In the physical model, water is supplied at the bottom of the plane, and the velocity profile of the water film is determined by two driving forces, gravity and wind drag. In a previous paper, a model of air/water/ice/aluminum multi-phase system was considered to explain an initial aufeis morphology [1]. In that model configuration, gravity magnifies the flow of supercooled water due to air shear stress. On the other hand, in the current model configuration, gravity impedes the effect of air shear stress. Differences in the ice surface roughness characteristics caused by this asymmetric configuration are considered, as well as the effect of ice surface roughness on the convective heat transfer coefficient at the water-air interface. Without employing any of the empirical methods used in the standard icing models, the convective heat transfer coefficient is calculated explicitly by solving the governing equations of the air/water/ice/aluminum multi-phase system.

1. INTRODUCTION

In a previous paper [1], a variety of aufeis (icings) morphologies with various surface features were investigated by combining two driving mechanisms due to gravity and wind drag. The morphological instability of the ice-water interface under the water film flow due to these two driving forces was also relevant to the surface roughness characteristics associated with glaze icing formation around aircraft wings and structures. However, in glaze icing conditions, the numerical results of ice accretion based on the conservation of energy and mass were in poor agreement with the experimental results. Most analyses on current glaze ice accretion models based on global energy balance lack the physical motivation to account for the effect of surface roughness on the heat transfer coefficient at the water-air interface, and for roughness, which is treated as input to the numerical codes. Therefore, a more microscopic energy balance and detailed analysis of the interaction between the air and water flows are necessary to calculate the heat transfer coefficient. The purpose of this paper is to consider the effect of surface roughness on the heat transfer coefficient for an air/water/ice/aluminum multi-phase system with different configurations.

2. RESULTS

The convective heat transfer coefficient at the water-air interface on roughed ice surface depends not only on the temperature gradient at the water-air interface, but also on the shape of the water-air interface. The undisturbed velocity profile of the water film depends on the direction of forces acting on the water film, causing different water thickness and ice morphologies. When estimating the heat transfer coefficient, the shape of the water-air interface must be correctly predicted by taking into account the effect of air shear stress disturbances on the water-air interface. Otherwise the resulting ice morphologies cannot be correctly predicted.

3. CONCLUSION

The effects of different configuration of air/water-ice/aluminum multi-phase system on the ice growth conditions were investigated. This was done with two configurations. The first one is when the water flow is driven by both air shear stress and gravity, which accelerated the flow. The other configuration is when the direction of these two forces is opposite. It was found that this asymmetry caused different ice morphologies even though the water supply rate, plane slope and air stream velocity were the same in both configurations. So, in order to extend the current two-dimensional planar model to practical aircraft and structural icing problems, the interactions among air, water and ice near the stagnation point of the objects must be considered. In this situation, the water flow rate, angle and air velocity change locally along the position of the objects. The method and concept developed in this paper can be applied to icing problems with more complex geometries.

4. REFERENCES

[1] K. Ueno and M. Farzaneh, “Roughness characteristics in aufeis morphology,” Proceedings of the 14th International Workshop on Atmospheric Icing of Structures, IWAIS, Chongqing, China, 4pp, 2011.

Convective heat transfer coefficient in air/liquid-water/ice/solid-wall multi-phase system

Kazuto Ueno and Masoud Farzaneh
NSERC/Hydro-Quebec/UQAC Industrial Chair on Atmospheric Icing of Power Network Equipment (CIGELE) and Canada Research Chair on Atmospheric Icing Engineering of Power Networks (INGIVRE), www.cigele.ca
Université du Québec à Chicoutimi, Chicoutimi, QC, Canada

***Abstract*— The physical model currently used in ice accretion codes is based on the conservation of energy and mass within numerical cells along the ice-accreting surface. This type of model works reasonably well in rime icing conditions. However, the results are much less satisfactory in glaze icing conditions because the interaction between the air flow and the unfrozen surface water dynamics is neglected. Although the surface film flow generates a rough ice surface, almost all glaze icing models lack the physical motivation for the ice surface roughness. Instead, roughness is treated as an input parameter in the model. In this paper, we consider a physical model of the water film flow over a rough ice surface on an aluminum substrate, taking into account the interaction between the air and water flows. In the physical model, water is supplied at the bottom of the plane, and the velocity profile of the water film is determined by two driving forces, gravity and wind drag. In a previous paper, a model of air/water/ice/aluminum multi-phase system was considered to explain an initial aufeis morphology [1]. In that model configuration, gravity magnifies the flow of supercooled water due to air shear stress. On the other hand, in the current model configuration, gravity impedes the effect of air shear stress. Differences in the ice surface roughness characteristics caused by this asymmetric configuration are considered, as well as the effect of ice surface roughness on the convective heat transfer coefficient at the water-air interface. Without employing any of the empirical methods used in the standard icing models, the convective heat transfer coefficient is calculated explicitly by solving the governing equations of the air/water/ice/aluminum multi-phase system.**

Keywords-convective heat transfer coefficient; surface roughness

I. INTRODUCTION

In a previous paper [1], a variety of aufeis (icings) morphologies with various surface features were investigated by combining two driving mechanisms due to gravity and wind drag [2]. The morphological instability of the ice-water interface under the water film flow due to these two driving forces was also relevant to the surface roughness characteristics associated with glaze icing formation around aircraft wings and structures. However, in glaze icing conditions, the numerical results of ice accretion based on the conservation of energy and mass were in poor agreement with the experimental results [3]. Most analyses on current glaze ice accretion models based on global energy balance lack the physical motivation to account for the effect of surface roughness on the heat transfer coefficient at the water-air interface, and for roughness, which is treated as input to the numerical codes. Therefore, a more microscopic energy balance and detailed analysis of the interaction between the air and water flows are necessary to calculate the heat transfer coefficient. The purpose of this paper is to consider the effect of surface roughness on the heat transfer coefficient for an air/water/ice/aluminum multi-phase system with different configurations.

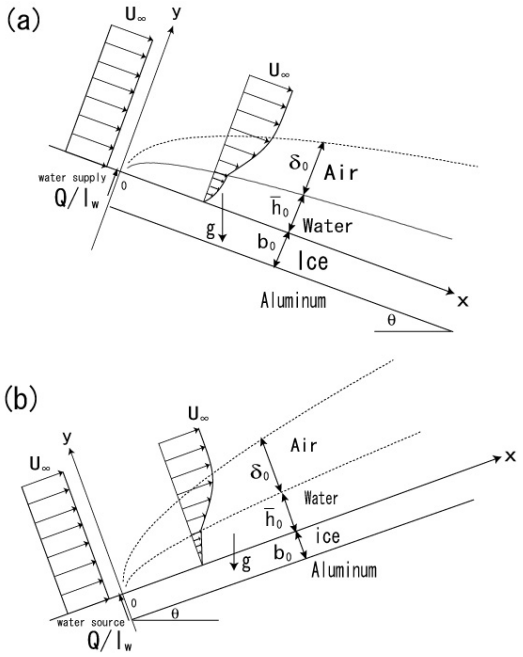

Figure 1. Schematic of model and coordinate system. (a) Gravity magnifies the effect of air shear stress. (b) Gravity impedes the effect of air shear stress.

II. MODEL

Since the basic theoretical framework herein is the same as that of a previous paper [1], details on the governing

equations are omitted and the readers are referred to that paper. The main difference between Figs. 1 (a) and (b) appears in the following equation:

$$\frac{\partial u_l}{\partial t}+u_l\frac{\partial u_l}{\partial x}+\mathrm{v}_l\frac{\partial u_l}{\partial y}=-\frac{1}{\rho_l}\frac{\partial p_l}{\partial x}+\nu_l\left(\frac{\partial^2 u_l}{\partial x^2}+\frac{\partial^2 u_l}{\partial y^2}\right)\pm g\sin\theta, \quad (1)$$

In the case of $+g\sin\theta$ in (1), gravity magnifies the effect of air shear stress, as shown in Fig. 1(a). On the other hand, in the case of $-g\sin\theta$ in (1), gravity impedes the effect of air shear stress, as shown in Fig. 1(b). The undisturbed part of (1) is given by

$$\nu_l\frac{d^2\bar{u}_l}{dy^2}\pm g\sin\theta=0, \quad (2)$$

which is subject to the following boundary conditions

$$\bar{u}_l\big|_{y=0}=0, \qquad \mu_l\frac{d\bar{u}_l}{dy}\bigg|_{y=h_0}=\mu_a\frac{d\bar{u}_a}{dy}\bigg|_{y=h_0}. \quad (3)$$

The solution of (2) is

$$\bar{u}_{l*}=\mp\frac{\bar{h}_0^2 g\sin\theta}{2\nu_l u_{la}}y_*^2+\left(\pm\frac{\bar{h}_0^2 g\sin\theta}{\nu_l u_{la}}+\frac{\mu_a u_\infty \bar{h}_0}{\mu_l u_{la}\delta_0}\frac{d^2\bar{F}_a}{d\eta^2}\bigg|_{\eta=0}\right)y_*, \quad (4)$$

where

$$u_{la}=\pm\frac{\bar{h}_0^2 g\sin\theta}{2\nu_l}+\frac{\mu_a u_\infty \bar{h}_0}{\mu_l\delta_0}\frac{d^2\bar{F}_a}{d\eta^2}\bigg|_{\eta=0} \quad (5)$$

is the surface velocity of the water film. Using (4), the water flow rate is given by

$$\begin{aligned} Q/l_w&=\int_0^{\bar{h}_0}\bar{u}_l dy=u_{la}\bar{h}_0\int_0^1\bar{u}_{l*}dy_* \\ &=\pm\frac{g\sin\theta}{3\nu_l}\bar{h}_0^3+\frac{\mu_a u_\infty}{2\mu_l\delta_0}\frac{d^2\bar{F}_a}{d\eta^2}\bigg|_{\eta=0}\bar{h}_0^2, \end{aligned} \quad (6)$$

where the plus sign of the first term of (6) is the case of Fig. 1(a), while the minus sign is that of Fig 1(b).

The current system is based on equations (21), (23), (24) with the boundary conditions (27), (28), (29) in the air, and (22), (25), (26) in the water film with the boundary conditions (30), (31) in the previous paper [1], as well as the cubic equation (6) for $\bar{h}_0$ in the present paper. For a given Q/l_w, θ, u_∞ and x, the value of $\bar{h}_0$ is numerically determined by solving (6). In the case of $u_\infty=20$ m/s, the term u_{la}/u_∞ in the boundary conditions in [1] can be neglected. The value $d^2\bar{F}_a/d\eta^2|_{\eta=0}$ in (6) is obtained by solving (21) subject to the boundary conditions (27) in [1]. f_a is obtained by solving (23) subject to the boundary conditions (28). By substituting the derived solutions $\bar{F}_a$ and f_a into (32) and (33), the tangential and normal air shear stress disturbances Σ_a and Π_a are calculated. Using these Σ_a and Π_a and boundary conditions (30), f_l is obtained from (25). H_a is solved from (24) with the boundary conditions (29), and the derived solutions H_a and f_l are substituted into (31). Using (31), H_l is solved from (26). Finally, the real part $H_l^{(r)}$ and imaginary part $H_l^{(i)}$ of the solution H_l are substituted into the dimensionless amplification rate and the dimensionless phase velocity for the disturbance of the ice-water interface [1]:

$$\sigma_*^{(r)}=-\frac{dH_l^{(r)}}{dy_*}\bigg|_{y_*=0}+K_l^s k_{l*}\frac{\cosh(k_{l*}b_0/\bar{h}_0)}{\sinh(k_{l*}b_0/\bar{h}_0)}\left(-G_l^s+H_l^{(r)}|_{y_*=0}-1\right), \quad (7)$$

$$\mathrm{v}_{p*}=-\frac{1}{k_{l*}}\left(-\frac{dH_l^{(i)}}{dy_*}\bigg|_{y_*=0}+K_l^s k_{l*}\frac{\cosh(k_{l*}b_0/\bar{h}_0)}{\sinh(k_{l*}b_0/\bar{h}_0)}H_l^{(i)}|_{y_*=0}\right). \quad (8)$$

The local convective heat transfer coefficient in current system is decomposed as $h_x=\bar{h}_x+h_x'$, where $\bar{h}_x=-K_a\partial\bar{T}_a/\partial y|_{y=\bar{h}_0}/(T_{la}-T_\infty)$ is the undisturbed part and $h_x'=\mathrm{Im}[-K_a\partial T_a'/\partial y|_{y=\bar{h}_0}/(T_{la}-T_\infty)]$ is the disturbed part, and where Im denotes the imaginary part of the argument. For laminar air flow, $\bar{h}_x=0.296K_a\sqrt{u_\infty/(\nu_a x)}$ [3] and

$$|h_x'|/\bar{h}_x=\left\{\left(G_a'^{(r)}f_l^{(r)}\big|_{y_*=1}-G_a'^{(i)}f_l^{(i)}\big|_{y_*=1}\right)^2+\left(G_a'^{(r)}f_l^{(i)}\big|_{y_*=1}+G_a'^{(i)}f_l^{(r)}\big|_{y_*=1}\right)^2\right\}^{1/2}, \quad (9)$$

where

$G_a'^{(r)}=\bar{h}_0/\delta_0(-dH_a^{(r)}/d\eta)\big|_{\eta=0}$, $G_a'^{(i)}=\bar{h}_0/\delta_0(-dH_a^{(i)}/d\eta)\big|_{\eta=0}$

and $f_l^{(r)}$, $f_l^{(i)}$ are real and imaginary parts of the disturbed temperature gradient at the water-air interface, $G_a'=\bar{h}_0/\delta_0(-dH_a/d\eta)\big|_{\eta=0}$, and f_l, respectively. It should be noted that without employing any of the empirical methods, $|h_x'|/\bar{h}_x$ can be calculated by substituting the solutions H_a and f_l for a given thickness δ_0 and $\bar{h}_0$.

III. Results

In the case of Fig. 1(a), there exists a water film for any values of Q/l_w because the solution of (6) is uniquely determined, as shown in Fig. 2(a). On the other hand, in the case of Fig. 1(b), there exists solutions of $\bar{h}_0$ to satisfy (6) only in a finite range of Q/l_w, as shown in Fig. 2(b). For

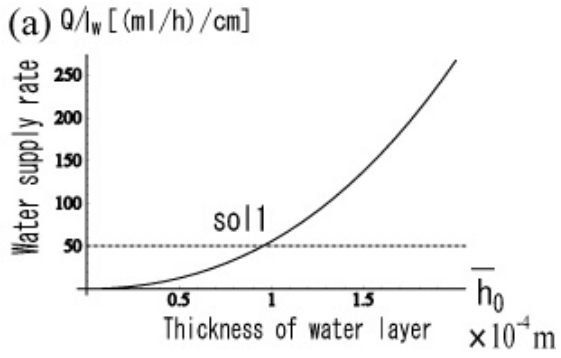

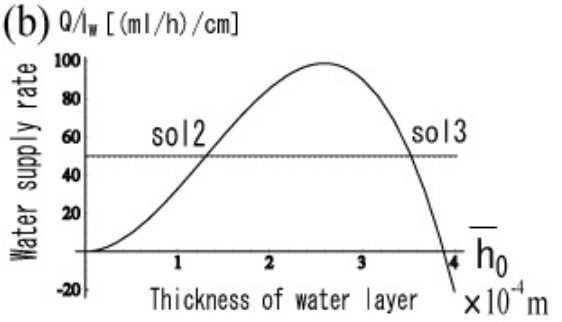

Figure2. Water rate per width, Q/l_w, and water film thickness $\overline{h}_0$. (a) and (b) represent the case in Fig. 1(a) and (b), respectively.

example, at $Q/l_w = 50$ [(ml/h)/cm], the thickness is $\overline{h}_0 = 0.95\times10^{-4}$m in Fig. 2(a), while $\overline{h}_0 = 1.31\times10^{-4}$m and $\overline{h}_0 = 3.5\times10^{-4}$ m in Fig. 2 (b). Henceforth, the solutions are referred to as sol1, sol2 and sol3. The corresponding velocity profiles, $\overline{u}_{l*}$, of the water film are shown in Fig. 3. In Fig. 3 (a), the profile is slightly protruding compared to the linear profile $\overline{u}_{l*} = y_*$ because the flow due to air shear stress is enhanced by gravity. On the other hand, in Fig. 3 (b), the profile is slightly depressed compared to the linear profile because the flow due to air shear stress is weakened by gravity. In Fig. 3(c), the water in the upper side flows upwards due to air shear stress, while the water in the lower side flows down due to gravity.

These asymmetries in the flow give rise to different ice roughness spacings. Figs. 4 (a), (b) and (c) show $\sigma_*^{(r)}$ against k_{a*} for each solution. For $b_0 = 100\delta_0$, the ice-water interface becomes unstable and $\sigma_*^{(r)}$ in Figs. 4 (a), (b) and (c) acquires a maximum value at $k_{a*} = 0.2$, 0.07, 0.02, respectively. The corresponding wavelength of surface roughness is $\lambda =$ 1.1, 3.2, 11.3 cm, and $v_p = -1.06\overline{V}$, $-0.14\overline{V}$, $-11.8\overline{V}$, respectively. These results indicate that the ice roughness spacing in the configuration of Fig. 1(a) is shorter than that of Fig. 1 (b). The thickness of the water film in Fig. 1(a) is less than that in Fig. 1(b). Therefore, ice roughness spacing is correlated

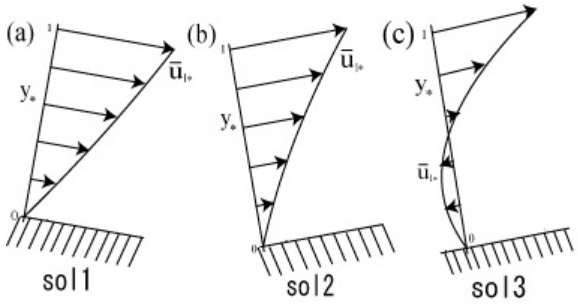

Figure 3. Velocity profiles of water film for (a) sol1, (b) sol2 and (c) sol3 in Fig. 2.

with the thickness of the water film, which depends on the water flow rate Q/l_w, plane slope θ and air stream velocity u_∞. On the other hand, for $b_0 = \delta_0$, the ice-water interface disturbance is stable for all wave numbers. In the present system, the latent heat is transferred to the air by convection and into the aluminum substrate by heat conduction. Fig. 4 indicates that when the ice thickness b_0

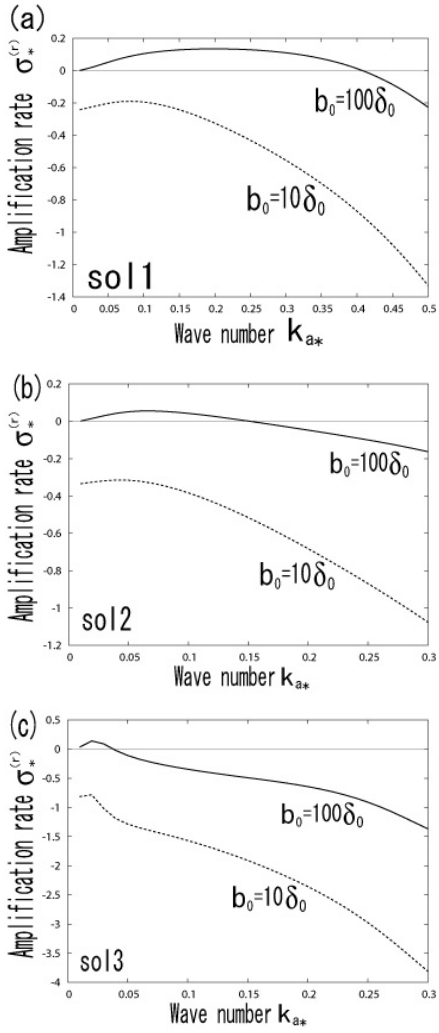

Figure 4. Dimensionless amplification rate vs. dimensionless wave number for (a) sol1 , (b) sol2 and (c) sol3.

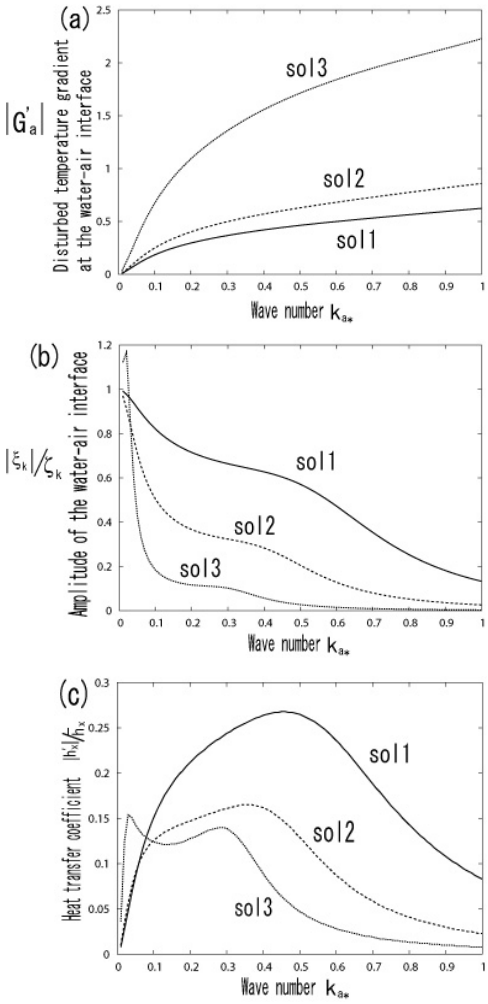

Figure 5. For sol1, sol2 and sol3 , (a) disturbed temperature gradient at the water-air interface vs. wave number k_{a^*}, (b) amplitude of the water-air interface vs. wave number, (c) the ratio of disturbed heat transfer coefficient to undisturbed heat transfer coefficient against the wave number. $k_{a^*} = 1$ corresponds to the wavelength of 2.3 mm.

is small during the growth most of the latent heat is conducted into the aluminum plate. In order for the ice-water interface to become unstable, the latent heat must be transferred to the air, which is realized for large ice thickness.

Figs. 5 (a), (b) and (c) show the disturbed temperature gradient at the water-air interface,

$$|G_a'| = \left\{ \left(G_a'^{(r)}\right)^2 + \left(G_a'^{(i)}\right)^2 \right\}, \tag{10}$$

the ratio of amplitude of the water-air interface to that of the ice-water interface,

$$|\xi_k| / \zeta_k = \left\{ \left(f_l^{(r)}\big|_{y_*=1} \right)^2 + \left(f_l^{(i)}\big|_{y_*=1} \right)^2 \right\}^{1/2}, \tag{11}$$

and the ratio of disturbed heat transfer coefficient to the undisturbed heat transfer coefficient, $|h_x'| / \bar{h}_x$, against wave number k_{a^*} for sol1, sol2 and sol3. $|G_a'|$ increases with increasing k_{a^*}, but $|\xi_k| / \zeta_k$ decreases with increasing k_{a^*} due to the effect of the surface tension on the water-air interface. As indicated in (9), $|h_x'| / \bar{h}_x$ depends not only on the disturbed temperature gradient at the water-air interface but also on the shape of the water-air interface. Therefore, if the shape of the water-air interface is not correctly calculated, the heat transfer coefficient cannot be correctly evaluated.

IV. Conclusions

The effects of different configuration of air/water-ice/aluminum multi-phase system on the ice growth conditions were investigated. This was done with two configurations. The first one is when the water flow is driven by both air shear stress and gravity, which accelerated the flow. The other configuration is when the direction of these two forces is opposite. It was found that this asymmetry caused different ice morphologies even though the water supply rate, plane slope and air stream velocity were the same in both configurations. So, in order to extend the current two-dimensional planar model to practical aircraft and structural icing problems, the interactions among air, water and ice near the stagnation point of the objects must be considered. In this situation, the water flow rate, angle and air velocity change locally along the position of the objects. The method and concept developed in this paper can be applied to icing problems with more complex geometries.

Acknowledgment

This study was carried out within the framework of the NSERC/Hydro-Québec/UQAC Industrial Chair on Atmospheric Icing of Power Network Equipment (CIGELE) and the Canada Research Chair on Engineering of Power Network Atmospheric Icing (INGIVRE) at the Université du Québec à Chicoutimi. The authors would like to thank all CIGELE partners (Hydro-Quebec, Hydro One, Réseau Transport d'Electricite (RTE) and Electricité de France (EDF), Alcan Cable, K-Line Insulators, Tyco Electronics, Dual-ADE, and FUQAC) whose financial support made this research possible.

References

[1] K. Ueno and M. Farzaneh, "Roughness characteristics in aufeis morphology," Proceedings of the 14th International Workshop on Atmospheric Icing of Structures, IWAIS, Chongqing, China, 4pp, 2011.

[2] J. T. Streitz and R. Ettema, "Observations from an aufeis windtunnel," Cold Reg. Sci. Technol, vol. 34, pp. 85–96, 2002.

[3] R. W. Gent, N. P. Dart, and J. T. Cansdale, "Aircraft icicng," Phils. Trans. R. Soc. London, Ser. A, vol. 358, pp.2873-2911, 2000.